

# Magnetic transition in marcasite FeTe<sub>2</sub> induced by the competition between crystal field splitting and Coulomb repulsion

Yue-Fei Hou<sup>1,2,6</sup>, Zhibin Shao<sup>3</sup>, Minghu Pan<sup>4,\*</sup>, Shiyang Wu<sup>5</sup>, Fawei Zheng<sup>5</sup>, Zhen-Guo Fu<sup>1,6,‡</sup>, and Ping Zhang<sup>1,6,7,†</sup>

<sup>1</sup>*Institute of Applied Physics and Computational Mathematics, Beijing 100088, China*

<sup>2</sup>*Graduate School, China Academy of Engineering Physics, Beijing 100088, China*

<sup>3</sup>*Physics Laboratory, Industrial Training Center, Shenzhen Polytechnic University, Shenzhen 518055, China*

<sup>4</sup>*School of Physics and Information Technology, Shaanxi Normal University, Xi'an 710119, China*

<sup>5</sup>*School of Physics, Beijing Institute of Technology, Beijing 100081, China*

<sup>6</sup>*National Key Laboratory of Computational Physics, Beijing 100088, China*

<sup>7</sup>*School of Physics and Physical Engineering, Qufu Normal University, Qufu 273165, China*

The determination of magnetic ground states in crystalline systems holds significant implications for both fundamental condensed matter physics and practical materials engineering. Marcasite-structured FeTe<sub>2</sub>, classified as a narrow-gap semiconductor, demonstrates anomalous magnetic behavior in low-temperature experimental investigations. This study employs first-principles density functional theory (DFT) calculations combined with scanning tunneling microscopy/spectroscopy (STM/STS) to elucidate the magnetic ground state of marcasite FeTe<sub>2</sub>. Our analysis reveals that the interplay between crystal field splitting and Coulomb repulsion critically governs the formation of localized magnetic moments in Fe ions. While bulk FeTe<sub>2</sub> is conclusively identified as non-magnetic in its ground state, we demonstrate that the previously observed magnetic responses originate from surface-localized magnetic Fe atoms in FeTe<sub>2</sub> specimens. This work establishes a robust yet straightforward criterion for determining ground-state magnetism across diverse localized electron systems, providing critical insights for interpreting magnetic phenomena in correlated electron materials.

-----  
\*Corresponding author. Email address: minghupan@snnu.edu.cn

‡Corresponding author. Email address: fu\_zhenguo@iapcm.ac.cn

†Corresponding author. Email address: zhang\_ping@iapcm.ac.cn

## I. Introduction

Marcasite  $\text{FeTe}_2$  is theoretically and experimentally confirmed to be a small-gap semiconductor, [1-6] yet the nature (direct or indirect) and the precise width of the energy gap remain to be definitively established. Experimental measurements also show that  $\text{FeTe}_2$  exhibits abundant magnetic features, [4-9] including room-temperature magnetism, antiferromagnetic exchange between magnetic moments, multiple magnetic phase transitions at different temperatures, and discernible magnetic anisotropy. These findings combine both magnetism and semiconductivity into  $\text{FeTe}_2$  and highlight the potential applications in spintronic devices. The magnetic properties of the ground-state  $\text{FeTe}_2$  are still debatable among different experimental studies which extend the measurements to near-zero temperature. Zhang et al. [4] and Du et al. [7] measured the magnetic susceptibility and their zero-field-cooling and field-cooling curves gave evidence for the antiferromagnetic (AFM) ground state of  $\text{FeTe}_2$ . Rahman et al. [5] measured temperature-dependent magnetization and resistivity, and a ferromagnetic (FM) ground state of  $\text{FeTe}_2$  was recommended. Moreover, the extrapolations of magnetization to zero temperature are also different among different groups of researchers [5, 7, 9], all showing the unsaturated feature of the magnetic moment. Given that the consistent crystal structure was indeed synthesized in these studies, the reason that causes the inconsistency of the magnetic measurements for ground-state  $\text{FeTe}_2$  is unclear. To contribute to both basic physics and potential applications, it is necessary to identify the magnetism of ground-state  $\text{FeTe}_2$  and provide the corresponding theoretical explanation.

In this work, we perform density functional theory (DFT) calculations and scanning tunneling microscopy/spectroscopy (STM/STS) to reveal the ground state of marcasite  $\text{FeTe}_2$ . In  $\text{FeTe}_2$  single crystal, the  $3d$  electrons are localized and with more orbital-like behaviors which introduces nodal lines or nodal planes of the electronic density. To reasonably describe this non-uniformity, the Perdew-Burke-Ernzerhof (PBE) type generalized gradient approximation (GGA)[10] is applied in our DFT calculations. The DFT plus Hubbard's  $U$  (DFT+ $U$ ) method [11] is adopted to include the on-site Coulomb interactions. In the experiment, the molecular beam epitaxy (MBE) method is adopted to prepare  $\text{FeTe}_2$  film on  $\text{SrTiO}_3$  substrate in an ultra-high vacuum, followed by annealing under a rich-Te atmosphere. STM/STS is used to show the atom-resolved bias-dependent images and the electronic density of states around the Fermi level of MBE-grown  $\text{FeTe}_2$  film. Based on these investigations, it is found that whether the Fe atoms in  $\text{FeTe}_2$  form localized magnetic moments or not, could be directly related to the competition between crystal field (CF) splitting and the Coulomb repulsion of the localized  $3d$  electrons. The ground state of  $\text{FeTe}_2$  bulk is confirmed to be nonmagnetic (NM) with a small indirect energy gap, while the surfaces of  $\text{FeTe}_2$  are spin-polarized with potential two-dimensional (2D) AFM orders. This picture of ground-state  $\text{FeTe}_2$  not only supports its semiconductivity but also explains that the uncertainty in measured saturated

magnetization [5, 7, 9] (in the unit of emu/g) may be caused by different ratios of surface to volume of different samples. Our work identifies a new example of Fe-based single crystal with quenched localized magnetic moments and shows the effectiveness of a highly simplified criterion in determining the localized moments.

## II. The STS gap and the localized magnetic moment criterion

Marcasite  $\text{FeTe}_2$  has an orthogonal structure with two Fe atoms and four Te atoms in the unit cell, as shown in Fig. 1(a). The group space is  $Pnmm(58)$ . The sample preparation was carried out in a molecular beam epitaxy chamber with a base pressure of  $3 \times 10^{-10}$  Torr. Firstly, the nearly monolayer FeTe films on the  $\text{SrTiO}_3$  substrate were grown. Subsequently, FeTe films were annealed under a rich-Te atmosphere for 15 minutes to obtain a rich-Te phase of  $\text{FeTe}_2$  compounds. As shown in Fig. 1(b), the STM observations show a clean and high-quality 010 surface of  $\text{FeTe}_2$  without reconstruction of the surface atoms. Through the measurements of the atomic distances on the 010 surface and the step height in the 010 direction of the crystal, the lattice parameters are determined to be  $a=3.75 \text{ \AA}$ ,  $b=5.4 \text{ \AA}$ , and  $c=6.1 \text{ \AA}$ . This is reasonably consistent with the X-ray diffraction (XRD) results.[5] As shown in Fig. 1(c), the STS spectrum shows the energy gap of  $\text{FeTe}_2$  for about 140 meV at the temperature of 4.2 K. At 77 K, the gap is maintained and slightly decreased to 95 meV due to the thermodynamic effects. The STS results report the small-gap semiconductivity of marcasite  $\text{FeTe}_2$  single crystal.

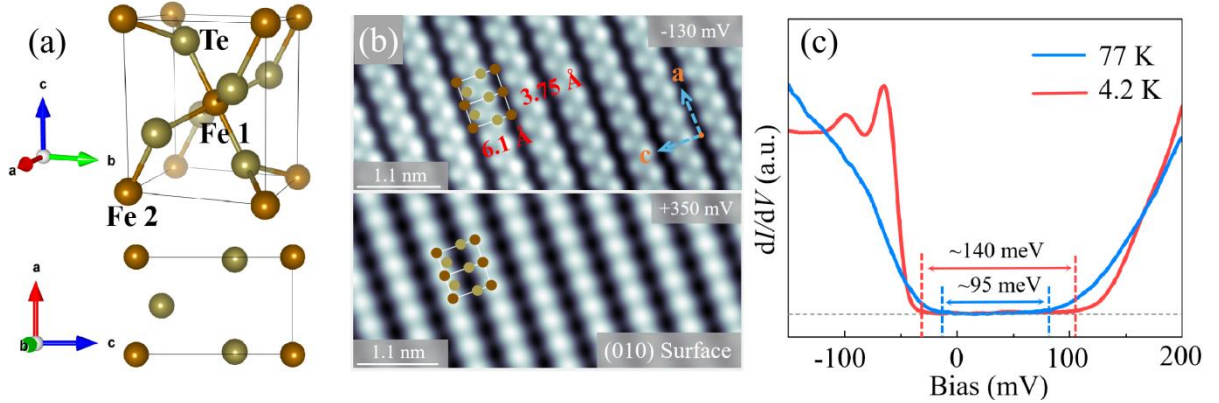


Figure 1 (a) The conventional cell of marcasite  $\text{FeTe}_2$  single crystal. (b) Atomic resolution images acquired at different biases, visualizing Te and Fe atomic layers of the 010 surface. Image sizes and scanning currents:  $5.6 \times 2.6 \text{ nm}^2$  and 200 pA. (c)  $dI/dV$  spectrums acquired at 4.2 K and 77 K. The dashed lines schematically mark the range of energy gap. Set Point:  $V_b = 300 \text{ mV}$ ,  $I_t = 200 \text{ pA}$ .

For an isolated Fe atom, the  $3d^6$  electronic configuration forms a total spin of  $S = 2$  according to Hund's rules. This feature is derived from both exchange interaction and Coulomb interaction. In  $\text{FeTe}_2$  crystal, whether the Fe atoms maintain the  $S = 2$  spin configuration, is additionally affected by the CF environment. In Fig. 2, a criterion is given to determine the  $3d^6$  spin configuration of the Fe

atoms based on single-electron approximation. If the CF splitting  $\Delta$  is large, a pair of electrons tend to occupy the same low-energy CF orbital to lower the total energy, although a Coulomb repulsion between the two paired electrons has to be tolerated. If the CF splitting  $\Delta$  is small, one of the paired electrons would make a transition to the high-energy CF orbital but release energy of  $U$ .  $U$  is the reduced Coulomb repulsive energy caused by changing double occupation on one orbital to single occupation on two different orbitals.

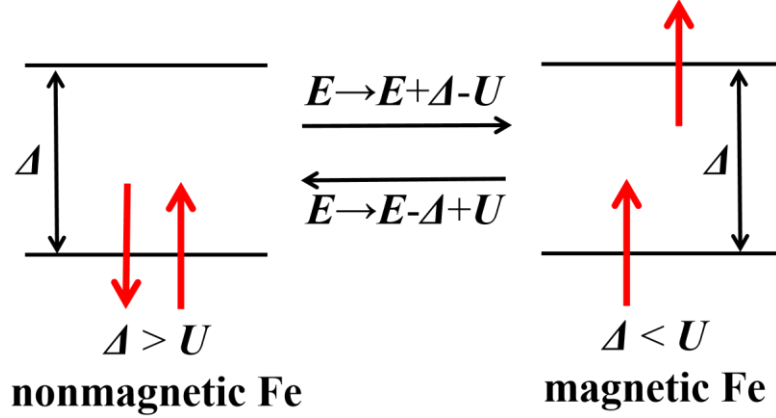


Figure 2 The criterion to judge the existence of localized magnetic moments in FeTe<sub>2</sub>.  $\Delta$  denotes the CF splitting and  $U$  denotes the Coulomb repulsion from the anti-parallel spins.

It is noteworthy that the criterion here can originate from Anderson's impurity mode. The Anderson's Hamiltonian has the form [12]

$$H = H_{\text{free}} + H_d + H_{\text{corr}} + H_{sd}. \quad (1)$$

As recommended by our STS and DFT results, the mixing between localized  $d$  and free electrons in gapped FeTe<sub>2</sub> is negligible. Hence the localized moments are only related to  $d$ -electron states and the Hamiltonian to determine localized moments reduces to

$$H = H_d + H_{\text{corr}}, \quad (2)$$

where the unperturbed Hamiltonian of the  $d$  electrons is

$$H_d = \sum_i \left[ -\frac{\hbar^2}{2m} \nabla_i^2 \right] + \sum_i V_i^{\text{CF}} + \frac{1}{2} \sum_{i,j} V_{ij}^{\text{ex}} \quad (3)$$

and the correlation energy is given by the Hubbard's model

$$H_{\text{corr}} = U n_{d\uparrow} n_{d\downarrow}. \quad (4)$$

On the right-hand side of Eq. (3), the first kinetic energy term is spin-independent, hence it is not included in the subsequent analysis. The second CF potential term can be reasonably simplified in an impurity model. For example in FeTe<sub>2</sub>, we consider the octahedral CF formed by the six nearest Te ligands around the Fe. As for the third exchange energy term, it can be absorbed into Eq. (4) by adopting a simplified Hubbard model [11] in our practical DFT+U calculations:

$$H_{\text{corr}} = \frac{(U-J)}{2} \sum_{\sigma} [\text{Tr} \rho^{\sigma} - \text{Tr}(\rho^{\sigma} \rho^{\sigma})] = \frac{U_{\text{eff}}}{2} \sum_{\sigma} [\text{Tr} \rho^{\sigma} - \text{Tr}(\rho^{\sigma} \rho^{\sigma})], \quad (5)$$

where  $J$  denotes the exchange energy in Eq. (3).  $\rho^{\sigma}$  is the density matrix of the localized  $d$  electrons with spin  $\sigma$  ( $\sigma=\uparrow$  or  $\downarrow$ ). By tuning the value of  $U_{\text{eff}}$  in DFT calculations, the computed results would be different, so that the strength of Coulomb repulsion on  $3d$  electrons could be determined by comparing the simulated results with the experimental results. To keep a concise form, the Hamiltonian to determine localized moments eventually becomes

$$H = \sum_i V_i^{\text{CF}} + U n_{d\uparrow} n_{d\downarrow}. \quad (6)$$

Therefore, for non-degenerate CF energy levels, we obtain the energy difference between the magnetic state and the NM state:

$$\begin{aligned} \Delta E &= E_d^{\uparrow\uparrow} - E_d^{\uparrow\downarrow} \\ &= (E_{\text{ground}}^{\uparrow} + E_{\text{excited}}^{\uparrow} + 0) - (E_{\text{ground}}^{\uparrow} + E_{\text{ground}}^{\downarrow} + U) \\ &= E_{\text{excited}}^{\uparrow} - E_{\text{ground}}^{\downarrow} - U \\ &= \Delta - U. \end{aligned} \quad (7)$$

It reaches the criterion sketched in Fig. 2.

### III. The nonmagnetic ground state of FeTe<sub>2</sub> bulk

With variable  $U_{\text{eff}}$  being applied, the simulated physical properties are shown in Fig. 3. As shown in Fig. 3(a), the cell volume increases along with the increasing  $U_{\text{eff}}$  for NM, FM, and AFM states. Although the applied GGA exchange-correlation functional has a potential to predict slightly larger lattice parameters than the real samples [13-15], the cell volumes for magnetic states (FM and AFM) deviate from the experimental results badly. Only the NM states are reasonably consistent with the experiments. By computing the total energies of different magnetic states, a first-order NM-AFM phase transition is verified when  $U_{\text{eff}}$  is close to 1.5 eV, as shown in Fig. 3(b). This feature can be explained by the criterion introduced in Fig. 2, that with the CF splitting being unchanged in FeTe<sub>2</sub>, a larger  $U_{\text{eff}}$  ( $> 1.5$  eV) drives the paired electrons to be spin-polarized. Thus the ground state becomes a magnetic state for a large  $U_{\text{eff}}$ . It is noticeable that the AFM state is always lower in energy than the FM states, which implies the AFM superexchange interactions between the magnetic sites in FeTe<sub>2</sub>.

The existence of an energy gap for a semiconductor should be objective for both experiments and DFT calculations. Our STS measurements recommend an energy gap of 140 meV for FeTe<sub>2</sub>. The widths of the gap for different states are simulated with different  $U_{\text{eff}}$  to locate the best value of  $U_{\text{eff}}$ . As shown in Fig. 3(c), the NM state has an increasing indirect gap along with the increasing  $U_{\text{eff}}$ , which can be qualitatively explained by Hubbard's model. However, the simulated magnetic states (FM 1, FM 2, and AFM) of FeTe<sub>2</sub> are all metallic with no gap. More details of the electronic structures for different magnetic states are given in the Supplemental Materials (SM) [16]. To be

reasonably consistent with the experimental result, the value of  $U_{\text{eff}}$  for DFT calculations is eventually determined to be 1.2 eV to best describe both the NM and gapped characteristics of ground-state FeTe<sub>2</sub>.

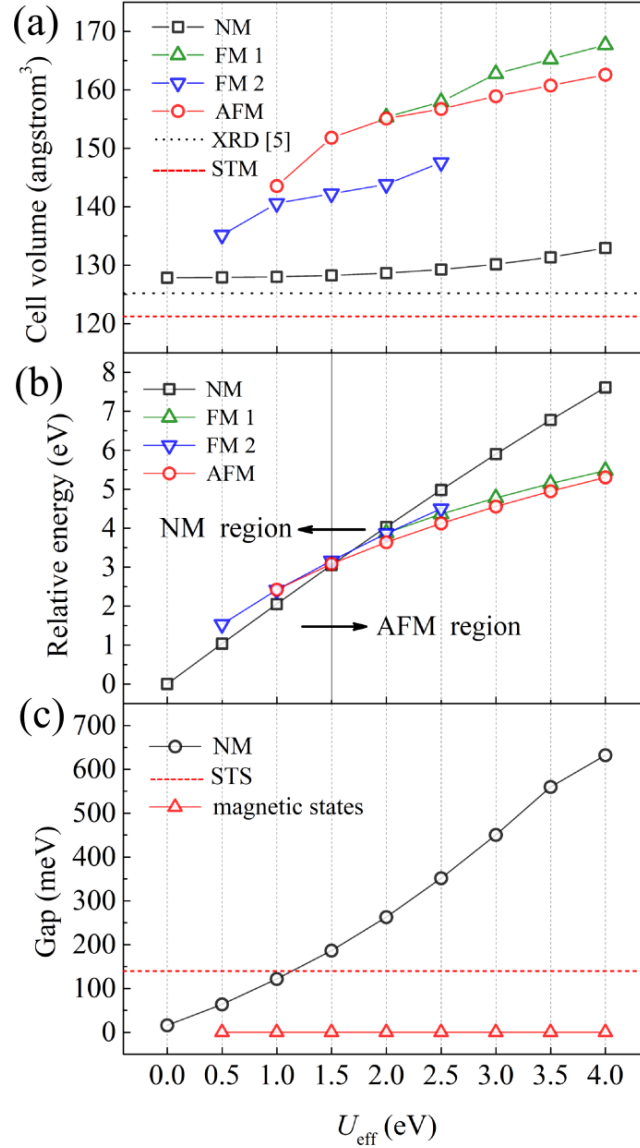


Figure 3 The simulated physical properties with different values of  $U_{\text{eff}}$ . (a) The volumes of the conventional cell for NM, FM, and AFM states. FM 1 and FM 2 are two different FM metastable states [16-18] with different  $3d$  localized orbital states. The XRD result [5] and our STM results are marked by the black dot line and the red dashed line, respectively. (b) The relative total energies for NM, FM, and AFM states. The NM-magnetic transition occurs at  $U_{\text{eff}} = 1.5$  eV. (c) The indirect energy gaps for NM and the magnetic states. Our STS gap is marked by the red dashed line.

Although both the XRD measurement [5] and our DFT calculations have observed small distortions of the FeTe<sub>6</sub> octahedral structure in FeTe<sub>2</sub>, the  $e_g - t_{2g}$  splitting in the strictly octahedral CF should be still partly maintained, as illustrated in Fig. 4 (a). According to the simulated results, the orbital-projected occupation numbers of each spin are 1.18 and 2.06 for  $e_g$  and  $t_{2g}$  orbitals,

respectively. These numerical results recommend the  $e_g^{\uparrow\downarrow}t_{2g}^{\uparrow\downarrow\uparrow\downarrow}$  spin state for the  $3d^6$  electronic configuration. While this is not totally consistent with the expected  $e_g^0t_{2g}^{\uparrow\downarrow\uparrow\downarrow\uparrow\downarrow}$  spin state in the limitations of both localized electrons and strictly octahedral CF, it still highlights the preference for  $t_{2g}$  orbital occupation. The corresponding electronic structure of the NM ground state is shown in Fig. 3(b). With  $U_{\text{eff}}$  being 1.2 eV, the indirect gap of FeTe<sub>2</sub> bulk is predicted to be 140 meV. Any magnetic ground states for FeTe<sub>2</sub> bulk are excluded by our DFT calculations due to the non-gapped feature. Spin-orbit coupling in FeTe<sub>2</sub> does not provide qualitative changes for the ground-state bands except for some reductions of the electronic degeneracy in the Brillouin Zone. In a word, it is proved by the DFT calculations that the CF splitting in FeTe<sub>2</sub> bulk wins the competition with Coulomb repulsion to form an NM ground state.

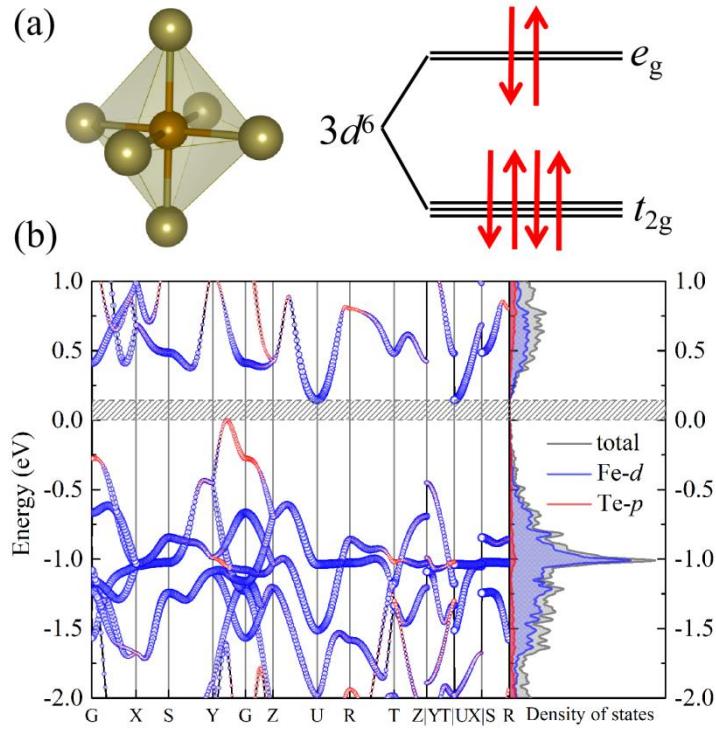


Figure 4 (a) The FeTe<sub>6</sub> octahedral structure with small distortions in FeTe<sub>2</sub> crystal and the electronic occupation of the  $3d^6$  configuration in the  $t_{2g}$ - $e_g$  splitting mode for the NM ground state of FeTe<sub>2</sub>. The six Te ligands form a distorted octahedral crystal field environment. (b) The electronic structure of the NM ground state of FeTe<sub>2</sub> with  $U_{\text{eff}} = 1.2$  eV. The width of the indirect gap is 140 meV. The contributions to the bands from Fe- $d$  and Te- $p$  orbitals are represented by blue and red circles, respectively.

#### IV. The magnetic feature on FeTe<sub>2</sub> surfaces

The CF splitting in FeTe<sub>2</sub> bulk is large enough to form the NM ground state as we have clarified. However, our DFT calculations show spontaneous spin polarization from the outermost Fe atoms on the surfaces of FeTe<sub>2</sub> bulk. As aperiodic boundaries, the type of the terminated atoms can be Fe, Te, or both of them (like 100 surface). We investigate the 010 surface and 001 surface of FeTe<sub>2</sub> in this work. These crystal surfaces only provide the Te-terminated (Te-T) surface or the Fe-terminated (Fe-T) surface. In the following part of the paper, we only discuss the 010 surface for simplicity, and

the results of the 001 surface are given in the SM [16]. The occupation numbers of the 3d shell are 6.48, 6.38, and 6.22 for Fe atoms from bulk, Te-T surface, and Fe-T surface, respectively. The corresponding localized spin magnetic moments are  $0 \mu_B$ ,  $1.3 \mu_B$ , and  $2.9 \mu_B$ , respectively. We can conclude from these numerical results that the occurrence of net spin is primarily due to the reconstruction of the spin state, but not the charge transfer of the 3d shell. Moreover, the computed differential charge density (figure shown in the SM) indicates a more covalent bonding feature between the Fe atoms and Te atoms. This also recommends that the localized 3d electrons of Fe hardly contribute to the Fe-Te bonding in  $\text{FeTe}_2$ .

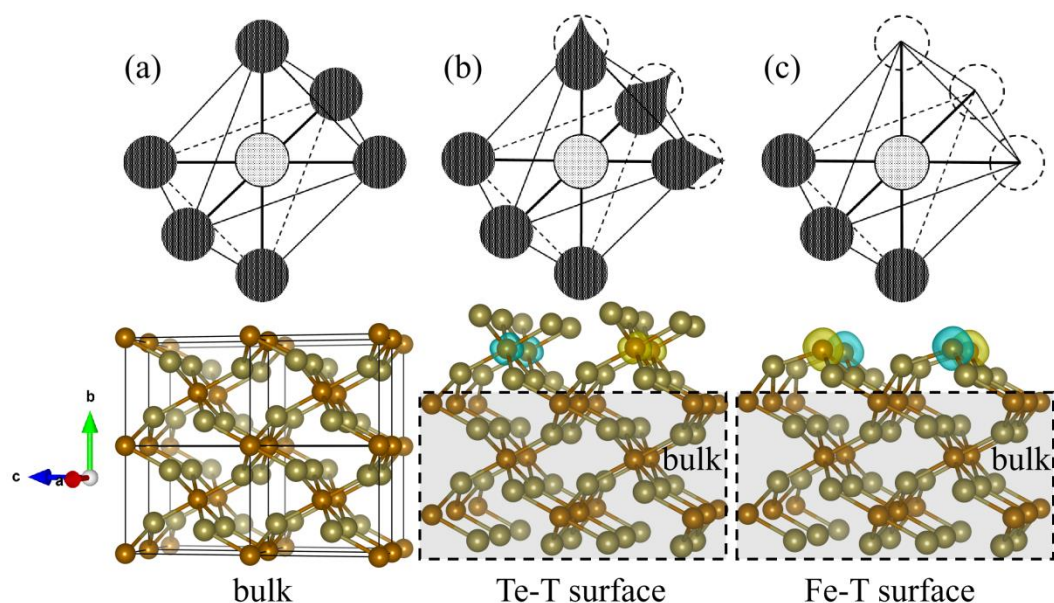


Figure 5 The breaking patterns of the octahedral CF and the corresponding spin densities for (a): bulk, (b): Te-T surface, and (c): Fe-T surface of  $\text{FeTe}_2$ . The dark spheres and the dark distorted spheres in the upper sketches represent the charge densities of the Te ligands. The yellow and blue isosurfaces in the lower sketches represent up spin density and down spin density, respectively.

Hence we point out that the magnetic feature of Fe on the surfaces primarily originates from the breaking of the octahedral CF formed by the six nearest Te ligands. The breaking patterns of the octahedral CF and the spin densities that imply local magnetic moments are shown in Fig. 5 (a), (b), and (c) for Fe in bulk, Fe on the Te-T surface, and Fe on the Fe-T surface, respectively. For Fe in bulk, the six ligands have nearly equal charge densities. The octahedral CF is thus with both the approximate symmetry of the  $O_h$  point group and a relatively large splitting  $\Delta$ . For Fe on the Te-T surface, three of its Te ligands which are on the surface, lack of attractive potential field from the vacuum side of the crystal surface. This different environment reshapes the charge densities of the three terminated Te atoms, which lowers the symmetry of the original octahedral CF for the central Fe. The CF splitting reduces to  $\Delta_1$  from  $\Delta$ , and the small net spin occurs according to the criterion. For Fe on the Fe-T surface, three of its Te ligands from the octahedron are removed. Not only the



symmetry of the CF is badly broken, but the strength of the CF potential is weakened. The CF splitting reduces to  $\Delta_2$  from  $\Delta_1$ , and  $\Delta_2$  should be much smaller than  $\Delta_1$  as well. The net spin of Fe on the Fe-T surface is thus larger than Fe on the Te-T surface. Since the maximum of the net spin magnetic moment can be  $4 \mu_B$  for Fe atoms, the unsaturated spin moments recommended by our DFT calculations imply residual CF strength for the surface Fe atoms.

Fig. 6 shows the simulated distribution for the localized magnetic moment of Fe controlled by  $U_{\text{eff}}$  and the strength of CF splitting. When  $U_{\text{eff}}$  is small in bulk FeTe<sub>2</sub>, with the strongest CF splitting, the localized moment of Fe is quenched. With the increase of  $U_{\text{eff}}$ , the NM-magnetic phase transition occurs at 1.5 eV. The localized moment then increases with the increase of  $U_{\text{eff}}$ . When the CF splitting is weakened on the Te-T surface or Fe-T surface of FeTe<sub>2</sub>, the localized moment can always exist and increase with the increase of  $U_{\text{eff}}$ . Note that the adopted PBE exchange-correlation functional naturally contains a portion of the electronic correlation effect. This provides enough Coulomb repulsive energy to form localized moments on the surfaces even if  $U_{\text{eff}}$  is zero. Now it can be concluded that the existence of localized magnetic moments on the surfaces of FeTe<sub>2</sub> is due to the victory of Coulomb repulsion in the competition with CF splitting.

The spin-polarized Fe atoms on the surface tend to form a 2D magnetic order due to the superexchange interactions mediated by Te atoms. By computing the total energies of the magnetic structures, the AFM structures are confirmed to have the lowest energies for both the Te-T surface and the Fe-T surface. The magnetic anisotropy of the magnetic Fe on the surfaces is also simulated. The notable magnetic anisotropy energies (MAEs) are recommended by our DFT calculations. The detailed data of the total energies of the magnetic structures and the MAEs are shown in the SM [16].

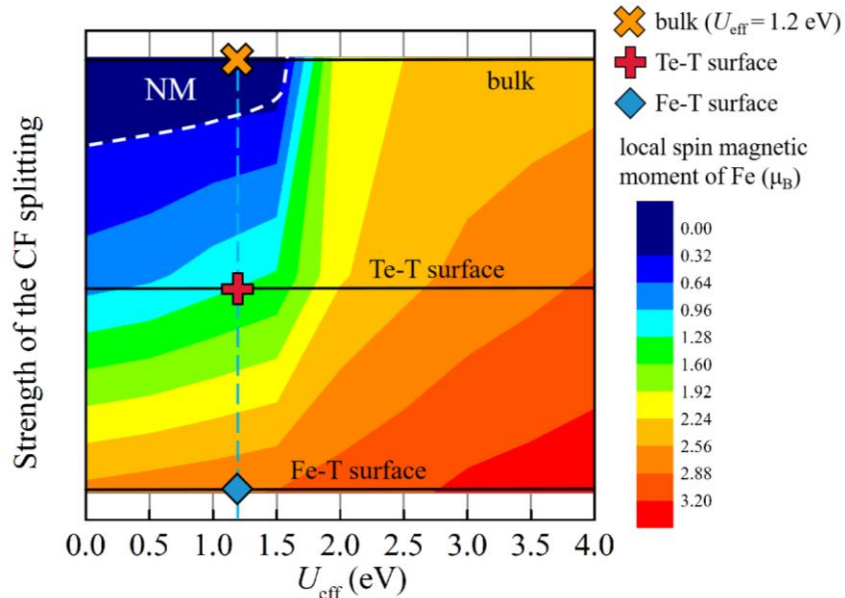


Figure 6 The distribution for localized magnetic moment of Fe controlled by  $U_{\text{eff}}$  and the strength of CF splitting. The NM phase of  $\text{FeTe}_2$  occurs at the left top corner of the phase diagram. The color distribution is achieved by making interpolations of the originally simulated points. There are three points vertically (bulk, Te-T surface, and Fe-T surface) and nine points horizontally (0-4 eV with a step of 0.5 eV).

## V. Discussions and conclusions

The ground state of  $\text{FeTe}_2$  is confirmed to be NM in bulk and AFM on the surfaces. This picture of  $\text{FeTe}_2$  can explain the abnormal experimental observations, such as the unsaturated magnetic moment of Fe measured in the unit of emu/g. In other words, the measurements of magnetization are not proper to determine the magnetic moment of Fe without the characterization of the shape of the sample, since most Fe atoms that contribute to the total mass in the bulk are NM. Moreover, given that the breaking CF helps to form localized moments, crystal surfaces, grain boundaries, and defects [19] may bring unexpected magnetic responses to  $\text{FeTe}_2$  and experimentally cause the deviation from typical magnetic systems. This highlights the significance of high-quality single-crystal samples in identifying the ground state of  $\text{FeTe}_2$ . A recent experiment for quasi-2D marcasite  $\text{FeTe}_2$  nanocrystal provides the thickness (about 10 nm) of their sample [9], which can be used to estimate the surface magnetic moment. Their measured magnetic moment is about  $0.043 \mu_B$  to  $0.064 \mu_B$  per Fe, showing a severely unsaturated feature. If our surface-magnetism picture is adopted, the estimated magnetic moment of the surface Fe atoms becomes about  $0.74 \mu_B$  to  $1.60 \mu_B$ , which are in the same order of magnitude as Fe on Te-T surfaces predicted by our DFT calculations. As a small-gap semiconductor, the potential magnetic orders at its surfaces or one-dimensional edges may also bring abundant in-gap states. The variable width of the gap at different surfaces and edges of  $\text{FeTe}_2$  has been detected by another STS study. [6] The correlation between surface magnetism and in-gap states makes  $\text{FeTe}_2$  a potential platform to explore exotic quantum states.

As a highly simplified model to determine localized magnetic moments, the criterion proposed in our study is based on single-electron approximation and the localized-electron limitation. Nonetheless, it is also expected that the criterion may be effective for metallic systems. Recently, we became aware of the arguments on the magnetic ground state of  $\text{RuO}_2$ . The metallic  $\text{RuO}_2$  single crystal was recognized as an altermagnetic (AM) candidate by polarized neutron diffraction [20], resonant x-ray scattering [21], and the angular distribution of photoelectrons [22]. However, the later ARPES[23], polarized neutron diffraction, and  $\mu\text{SR}$  spectroscopy [24, 25] identified the NM ground state of  $\text{RuO}_2$ . Smolyanyuk et al. [26] performed DFT calculations to investigate the magnetism of  $\text{RuO}_2$  and found an NM-AM transition with the increase of  $U_{\text{eff}}$ . Meanwhile, their computed electronic density of states of the Ru-4d orbitals show noticeable  $e_g-t_{2g}$  CF splitting caused by the  $\text{RuO}_6$  octahedral structure. We reproduced these results and eventually confirmed the similar competition

between CF splitting and Coulomb repulsion in RuO<sub>2</sub>. The detailed discussions regarding RuO<sub>2</sub> will be presented in our subsequent work.

In this work, DFT calculations and scanning tunneling microscopy/spectroscopy are applied to study the magnetic ground state of marcasite FeTe<sub>2</sub> single crystal. A theoretical criterion on the competition between crystal field splitting and Coulomb repulsion is proposed to judge the existence of the localized magnetic moments in FeTe<sub>2</sub>. The results of DFT calculations support the criterion and recommend that the FeTe<sub>2</sub> bulk is NM while the FeTe<sub>2</sub> surfaces are magnetic. This picture of the ground-state FeTe<sub>2</sub> also provides a view to explain abnormal phenomena in the magnetic measurements for other CF-Coulomb-competing systems.

### Acknowledgments

This work is supported by the National Key R&D Program of China (2022YFA1403100, 2022YFA1403101 and 2022YFA1403103), National Natural Science Foundation of China (No. 12275031 and 22372096), Shenzhen Polytechnic Research Fund (No. 6023310019K and 6022312037K), and Post-doctoral Later-stage Foundation Project of Shenzhen Polytechnic University (No. 6023271020K).

### References

- [1] Landolt-Börnstein (New Series), ed. K. H. Hellwege, Springer Verlag, Berlin, Heidelberg, New York, 1971, vol. III/6.
- [2] A. Mami, K. B. Messaoud, O. Kamoun, and M. Amlouk, *Journal of Materials Science: Materials in Electronics*. Springer (2019).
- [3] V. K. Gudelli, V. Kanchana, G. Vaitheeswaran, M. C. Valsakumar, and S. D. Mahanti, Thermoelectric properties of marcasite and pyrite FeX<sub>2</sub> (X = Se, Te): a first principle study, *RSC Adv.* **4**, 9424 (2014).
- [4] J. Zhang, B. Wu, C. J. O'Connor and W. B. Simmons, Magnetic characterization of amorphous intermetallic materials MTe<sub>2</sub> (M=Fe and Co), *J. Appl. Phys.* **73**, 5718–5720 (1993).
- [5] A. Rahman, D. Zhang, M. U. Rehman, M. Zhang, X. Wang, R. Dai, Z. Wang, X. Tao, and Z. Zhang, Multiple magnetic phase transitions, electrical and optical properties of FeTe<sub>2</sub> single crystals, *J. Phys.: Condens. Matter* **32**, 035808 (2020).
- [6] Z. Zhang, M. Cai, R. Li, F. Meng, Q. Zhang, L. Gu, Z. Ye, G. Xu, Y. Fu, and W. Zhang, Controllable synthesis and electronic structure characterization of multiple phases of iron telluride thin films, *Phys. Rev. Mater.* **4**, 125003 (2020).

- [7] J. Du, F. Wang, L. Jin, Z. Quan, Y. Bai, and X. Xu, Enhancement of ferromagnetism in FeTe<sub>2</sub> nanoparticles by Cr doping, *Materials Letters* **184**, 261–264 (2016).
- [8] A. Liu, X. Chen, Z. Zhang, Y. Jiang, and C. Shi, Selective synthesis and magnetic properties of FeSe<sub>2</sub> and FeTe<sub>2</sub> nanocrystallites obtained through a hydrothermal co-reduction route, *Solid State Communications* **138**, 538–541 (2006).
- [9] B. P. Jena and C. Sudakar, Micron-sized 2D marcasite FeTe<sub>2</sub> nanocrystals for spintronics applications, *ACS Appl. Nano Mater.* **7**, 26215–26225 (2024).
- [10] J. P. Perdew, K. Burke, and Y. Wang, Generalized gradient approximation for the exchange-correlation hole of a many-electron system, *Phys. Rev. B* **54**, 16533 (1996).
- [11] S. L. Dudarev, G. A. Botton, S. Y. Savrasov, C. J. Humphreys, and A. P. Sutton, Electron-energy-loss spectra and the structural stability of nickel oxide: An LSDA+U study, *Phys. Rev. B* **57**, 1505 (1998).
- [12] P. W. Anderson, Localized magnetic states in metals, *Phys. Rev.* **124**, 1 (1961).
- [13] J. P. Perdew, A. Ruzsinszky, G. I. Csonka, O. A. Vydrov, G. E. Scuseria, L. A. Constantin, X. Zhou, and K. Burke, Restoring the Density-Gradient Expansion for Exchange in Solids and Surfaces, *Phys. Rev. Lett.* **100**, 136406 (2008).
- [14] B. Sun, P. Zhang, and X. Zhao, First-principles local density approximation + U and generalized gradient approximation + U study of plutonium oxides, *The Journal of Chemical Physics* **128**, 084705 (2008).
- [15] Y. Hou, W. Jiang, S. Li, Z. Fu, and P. Zhang, Magnetic ground state of plutonium dioxide: DFT+U calculations, *Chin. Phys. B* **32**, 027103 (2023).
- [16] More details of each section in the study are given in the supplemental materials:
- [17] J. P. Allen and G. W. Watson, Occupation matrix control of d- and f- electron localisations using DFT+U, *Phys. Chem. Chem. Phys.* **16**, 21016 (2014).
- [18] Y. Hou, S. Li, X. Yang, W. Jiang, Q. Wang, F. Zheng, Z. Fu, and Ping Zhang, Magnetic ground state of monolayer CeI<sub>2</sub>: Occupation matrix control and DFT+U calculations, *Phys. Rev. B* **110**, 224421 (2024).
- [19] X. Tian, J. Zhang, X. Wei, and Y. Huang, Effects of intrinsic point defects on the structural, electronic, magnetic, and optical properties of marcasite FeS<sub>2</sub>, *Solid State Communications* **307**, 113808 (2020).
- [20] T. Berlijn, P. C. Snijders, O. Delaire, H.-D. Zhou, T. A. Maier, H.-B. Cao, S.-X. Chi, M. Matsuda, Y. Wang, M. R. Koehler, P. R. C. Kent, and H. H. Weitering, Itinerant antiferromagnetism in RuO<sub>2</sub>, *Phys. Rev. Lett.* **118**, 077201 (2017).
- [21] Z. H. Zhu, J. Stremper, R. R. Rao, C. A. Occhialini, J. Pellicciari, Y. Choi, T. Kawaguchi, H. You, J. F. Mitchell, Y. Shao-Horn, and R. Comin, Anomalous antiferromagnetism in metallic RuO<sub>2</sub> determined by resonant X-ray Scattering, *Phys. Rev. Lett.* **122**, 017202 (2019).

- [22] O. Fedchenko, J. Minár, A. Akashdeep, S. W. D'Souza, D. Vasilyev, O. Tkach, L. Odenbreit, Q. Nguyen, D. Kutnyakhov, N. Wind, L. Wenthaus, M. Scholz, K. Rosnagel, M. Hoesch, M. Aeschlimann, B. Stadtmüller, M. Kläui, G. Schönhense, T. Jungwirth, A. B. Hellenes, G. Jakob, L. Šmejkal, J. Sinova, H. Elmers, Observation of time-reversal symmetry breaking in the band structure of altermagnetic RuO<sub>2</sub>, *Sci. Adv.* **10**, eadj4883 (2024).
- [23] J. Liu, J. Zhan, T. Li, J. Liu, S. Cheng, Y. Shi, L. Deng, M. Zhang, C. Li, J. Ding, Q. Jiang, M. Ye, Z. Liu, Z. Jiang, S. Wang, Q. Li, Y. Xie, Y. Wang, S. Qiao, J. Wen, Y. Sun, and D. Shen, Absence of Altermagnetic Spin Splitting Character in Rutile Oxide RuO<sub>2</sub>, *Phys. Rev. Lett.* **133**, 176401 (2024).
- [24] P. Keßler, L. Garcia-Gassull, A. Suter, T. Prokscha, Z. Salman, D. Khalyavin, P. Manuel, F. Orlandi, I. I. Mazin, R. Valentí and S. Moser, Absence of magnetic order in RuO<sub>2</sub>: insights from  $\mu$ SR spectroscopy and neutron diffraction, *npj Spintronics* **2**, 50 (2024).
- [25] M. Hiraishi, H. Okabe, A. Koda, R. Kadono, T. Muroi, D. Hirai, and Z. Hiroi, Nonmagnetic ground state in RuO<sub>2</sub> revealed by Muon spin rotation, *Phys. Rev. Lett.* **132**, 166702 (2024).
- [26] A. Smolyanyuk and I. I. Mazin, Fragility of the magnetic order in the prototypical altermagnet RuO<sub>2</sub>, *Phys. Rev. B* **109**, 134424 (2024).